ELSEVIER

Polymer 42 (2001) 9447–9453

polymer

www.elsevier.com/locate/polymer

Influence of the electropolymerisation time on the nucleation mechanism, structure and morphology of polyfurane/perchlorate doped films

I. Carrillo[a,*], E. Sánchez de la Blanca[b], M.J. González-Tejera[b]

[a]*Dpto. Química Industrial y Polímeros, E.U.I.T. Industrial, Universidad Politécnica de Madrid, C/. Ronda de Valencia 3, 28012 Madrid, Spain*
[b]*Dpto. Química Física I, Facultad de Ciencias Químicas, Universidad Complutense, 28040 Madrid, Spain*

Received 5 April 2001; received in revised form 28 May 2001; accepted 2 July 2001

Abstract

The influence of electropolymerisation time, t_p, on the synthesis, structure and morphology of polyfurane films doped with perchlorate anions, PFu/ClO_4, was analysed. The analysis of the nucleation mechanism revealed a mixture of progressive and instantaneous nucleation of small hemispherical nodules controlled by spherical diffusion.

The morphological study revealed an ordered nodular structure and different levels of growth from the first seconds of synthesis untill higher t_p values. Dendritic formations on the growth face and the cross-section pores implied alternating planar and normal growth of the films.

FTIR spectra study verified that the structure of these polymers was influenced by t_p, so that the film aromaticity differed according to this parameter.

Keywords: Polyfurane; Electropolymerisation; Morphology

1. Introduction

In the last 30 years there has been a significant interest in conducting polymers, in the electropolymerisation parameters and in various properties associated with the mechanism of nucleation and growth and the morphology of films [1–5]. In spite of the differences among metal electrocrystallisation and electropolymerisation processes, we used electrochemical data to provide information on the first states of the polymer generation. The electrocrystallisation theory has been applied to the generation of polyfurane [6], polypyrrole [2,3,7–9], polythiophene and derivatives [10–12], polyaniline [13,14], polyparaphenylene [15] and poly-*N*-methylpyrrole [16].

Taking into account of the fact that the electropolymerisation time, t_p, influences several subjects such as nucleation and growth of the polymeric phase, the grade of length chain, ring rupture of the heterocyclic monomers and the order/disorder relationship in the polymeric structure, we analysed the current response to a controlled potential perturbation at different applied times from 1 to 6000 s in the synthesis of polyfurane films doped with perchlorate anions (PFu/ClO_4). The electrochemical results were used in conjunction with infrared spectra and SEM micrographs.

2. Experimental

Polyfurane films doped with perchlorate anions, PFu/ClO_4, were potentiostatically generated onto platinum electrodes at $\eta_p = 2.55$ V (Ag/Ag^+) at different electropolymerisation times ($t_p = 1$, 4, 10, 358, 600, 1200 and 6000 s) in non-aqueous electrolytic medium. The monomer furane, Fu (Aldrich Chemie, 99%), was distilled under vacuum before use. The non-aqueous electrolytic medium consisted of acetonitrile (MeCN) (Carlo Erba, RPE quality) dried over 3 Å molecular sieves, and sodium perchlorate ($NaClO_4$) (Aldrich Chemie, 99%). Both Fu and $NaClO_4$ concentrations were 0.1 M. A PAR273A potentiostat/galvanostat was used, controlled by PAR Model 270/250 Research Electrochemistry Software 4.00. Details of the electrosynthesis are described elsewhere [17,18].

Each PFu/ClO_4 film is designated by the letter A and a subscript, which indicates the t_p value in the film generation (i.e. A_1, A_4,…, A_{6000}).

FTIR spectra were obtained at room temperature in the region 4000–400 cm^{-1} using a NICOLET 60SX Fourier transform interferometer equipped with a DTGS detector.

* Corresponding author. Tel.: +34-91-336-3223; fax: +34-91-336-6836.
E-mail address: icarrillo@qi.upm.es (I. Carrillo).

0032-3861/01/$ - see front matter
PII: S0032-3861(01)00500-6

All spectra were recorded at 1 cm^{-1} resolution and 32 scans were averaged to improve the signal/noise ratio. The instrument was purged with dry air. Infrared spectra were registered from pressed discs of each PFu/ClO_4 sample mixed with KBr powder. The background (air + KBr) spectrum was removed by subtracting from the film spectra.

Scanning electron micrographs were obtained on a JEOL model JSM 6400 electron microscope at 20 kV by varying the levels of magnification. Samples were sputter-coated with a thin gold film to avoid charge build-ups. Both the faces and the cross-section, which corresponded to a transverse fracture of the film, were examined. The working electrode was polished before each electrodeposition to avoid any specific orientation. More details of sample preparation can be found elsewhere [19,20]. A Videoplan image programme was used to determine the average area and perimeter of the nodules of the film surface and pores of the internal structure.

3. Results

3.1. Electrochemical study

Fig. 1 shows the first 35 s of the synthesis of PFu/ClO_4 films. It was necessary to apply unless a value of $t_p = 358$ s to completely cover both the electrode faces, At $t_p \leq 10$ s only the four edges of the working electrode were covered. At shorter, times the j–t_p transients show the characteristic regions described in Ref. [6]: a maximum current (A) when the potential jump is applied followed by a rapid decrease of the current density, minimum B (t_0, j_0). The coordinates t_0 and j_0 represent the time and current density from which the nucleation and growth of nuclei begin due to the generation of an oligomeric fraction producing a supersaturated layer close to the electrode [21]. After the minimum (B), the chronoamperograms showed an increase in the current density tending towards the maximum C. The nucleation and growth of the film took place in this period of time. After the maximum (C), at longer times (not visible in Fig. 1), the current density slowly decreased due to diffusion of the monomeric and oligomeric fractions.

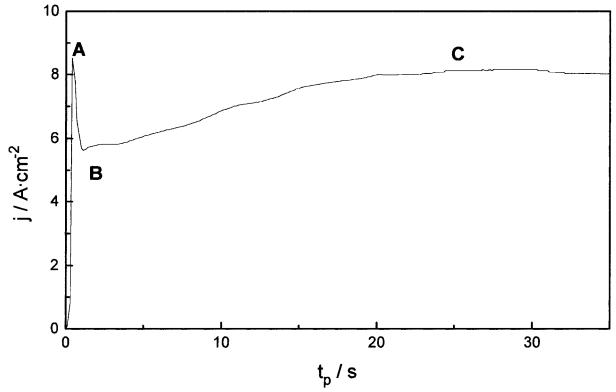

Fig. 1. Chronoamperogram of PFu/ClO_4 films obtained at $t_p = 600$ s.

The rate of charge consumption, $j_p = \Delta Q_p/\Delta t_p$, for each t_p value was evaluated by the plot of Q_p vs. t_p. In all films analysed, there was a change in the slope of these plots from 7 to 2.5 mC cm^{-2} s^{-1}, although the same order of magnitude was maintained, indicating that the formation rate of the polymer film was almost constant.

In order to evaluate the nucleation and growth mechanism in films synthesised at $t_p \geq 358$ s, we subtracted the corresponding minimum coordinates (t_0, j_0) to eliminate the effect of the initial diffusion process. The Avrami theorem may be applied with a reasonable level of confidence, considering the overlapping detected by the morphological study, to a three-dimensional growth of hemispherical nuclei randomly distributed on the electrode surface [6]. Given that it is difficult to distinguish between the different nucleation mechanisms, instantaneous or progressive, we must admit the possibility that both mechanisms could occur simultaneously. So all the experimental data for each t_p were fitted assuming both [22]

$$j(t) = \frac{nFD^{1/2}c^0}{\pi^{1/2}t^{1/2}}\left[(1 - \exp(-N_0\pi kDt)) + \left(1 - \exp - \frac{AN_o\pi k'Dt^2}{2}\right)\right] \quad (1)$$

where $k = (8\pi c^0 M/\rho)^{1/2}$; $k' = 4/3(8\pi c^0 M/\rho)^{1/2}$; c^0, electrolyte concentration in the bulk solution (mol cm^{-3}); F, Faraday constant (C mol^{-1}); D, diffusion coefficient (cm^2 s^{-1}); M, molecular weight (g mol^{-1}); N_0, number of sites where the nucleation can occur (cm^{-2}); ρ, density (g cm^{-3}); A, rate constant for nucleus formation.

Fig. 2 shows our experimental results for A_{600}, the total fit according to Eq. (1) and the fit of separate contributions to the nucleation mechanism. In these synthesis conditions the progressive contribution prevails to the instantaneous

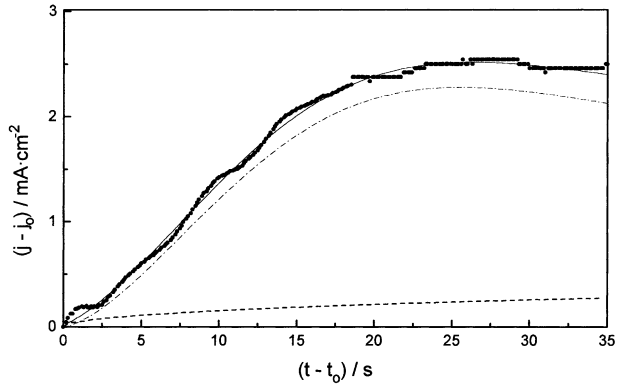

Fig. 2. Plots of ($j - j_o$) vs. ($t - t_o$) according to Eq. (1) (—). Experimental data of A_{600} film (●). Contribution of instantaneous nucleation (- - -) and progressive nucleation (– · –). These were calculated from the respective terms of Eq. (1).

nucleation, although at very short times, it seems that both mechanisms contribute in the same way.

3.2. Infrared study

The infrared study focused on films synthesised at $t_p \geq 358$ s when the electrode was completely covered. At lower t_p values, $t_p = 1$, 4 and 10 s, the film was so thin that there was not enough material for infrared analysis. Fig. 3 shows the FTIR spectra (4000–400 cm^{-1}) for A_{600} films.

The PFu/ClO_4 film spectra presented the same bands as were observed in other PFu/ClO_4 films synthesised in different conditions [23]. In the high frequency region the OH, $CH_{aromatic}$ and $CH_{aliphatic}$ stretching vibrations centered at about 3500, 3133 and 3000 cm^{-1}, respectively, were observable. In the 2000–400 cm^{-1} region the C=O stretching (1700 cm^{-1}), the combination band of C=C aromatic ring stretching and ring deformation (1550 cm^{-1}) and the combination band of ring deformation and $C{=}C_{ring}$ stretching (1400 cm^{-1}) vibrations were observed. The CH out of plane bending vibration γ(CH) appeared as a weak band in the 800 cm^{-1} region. The strong absorption of the $NaClO_4$, due to Cl–O stretching vibration prevented analysis of this region.

To discount the contribution of $NaClO_4$, its FTIR spectrum was subtracted from each PFu/ClO_4 film spectrum (Fig. 4). The subtraction took into account two bands, one around 1120 cm^{-1} (Cl–O stretching vibration) and the other around 625 cm^{-1} (OClO in plane bending vibration). The absence of these bands on the PFu/ClO_4 subtracted spectra was used as a normalising factor.

In the high frequency region, the relative intensity of the $CH_{aromatic}$ stretching vibration was greater than the $CH_{aliphatic}$ stretching vibration. This indicated a larger proportion of aromatic than aliphatic groups in all the spectra studied, in spite of the ring rupture confirmed by the presence of OH stretching vibration. The CH aromatic proportion increased with t_p until 1800 s; from this t_p on, the CH aromatic decreased. A similar effect with t_p was observed in the combination band due to the ring deformation and $C{=}C_{ring}$ stretching vibration (at 1400 cm^{-1}).

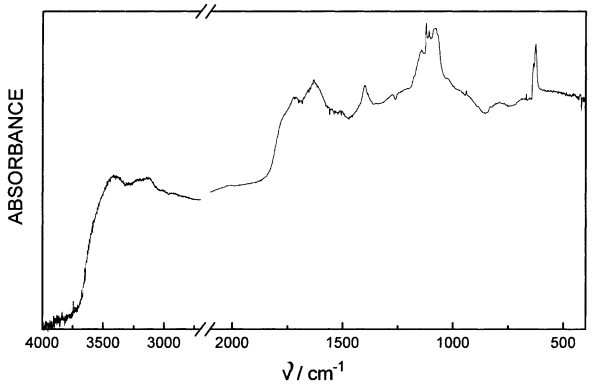

Fig. 3. FTIR spectra of A_{600} films (4400–400 cm^{-1}).

In A_{4400} film there was a negative band at the same frequency, which could be attributed to an 'Evans hollow' [24]. Evans asserts that these negative bands appear when a deformation normal vibration, that gives wide bands, interacts with other normal vibrations corresponding to fundamental groups, producing a narrow band between them. The wide bands could be due to the OH group deformation or stretching vibration corresponding to the strong hydrogen bonding. These bands are observed in the spectra of solids that have hydrogen bonding OH···O shorter than 2.160 Å [25], giving a wide absorption band between 1800 and 600 cm^{-1}. The shift to low frequencies of the OH band seems to confirm this supposition. The same effect has been observed in other conducting polymers such us polyaniline [25]. At the same time, the 1400 cm^{-1} band decreased, which could indicate that the aromaticity diminished from this t_p upwards, and confirms the prediction made in the high frequency region. This effect was better observed after the subtraction of $NaClO_4$ (Fig. 4). Therefore, the analysis of FTIR spectra reveals some changes of the film structure with t_p.

3.3. Morphological study

The initial covering of the electrode's top edge during the

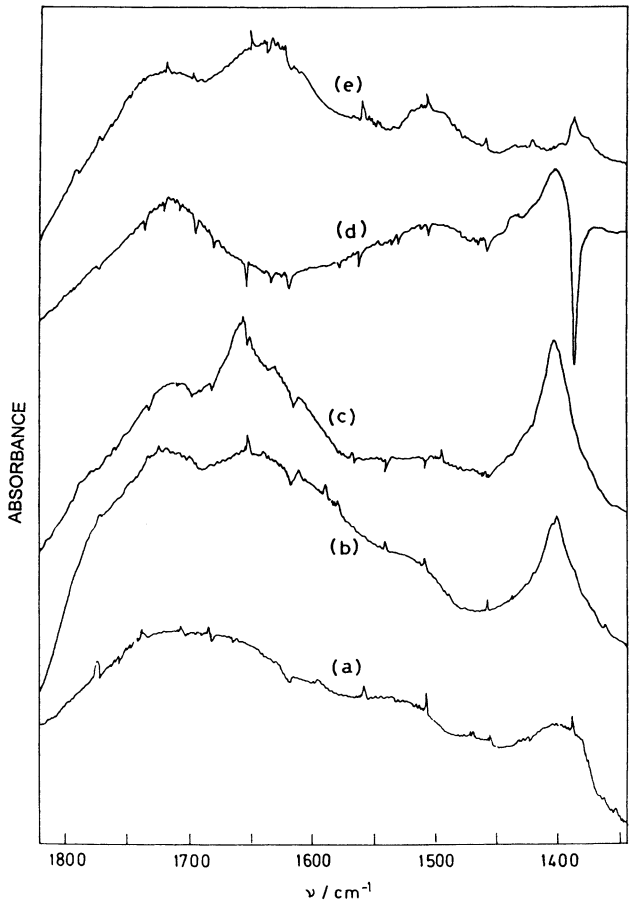

Fig. 4. FTIR spectra of PFu/ClO_4 films (2000–400 cm^{-1}) after subtraction of $NaClO_4$: (a) A_{358}, (b) A_{600}, (c) A_{1800}, (d) A_{4400} and (e) A_{6000}.

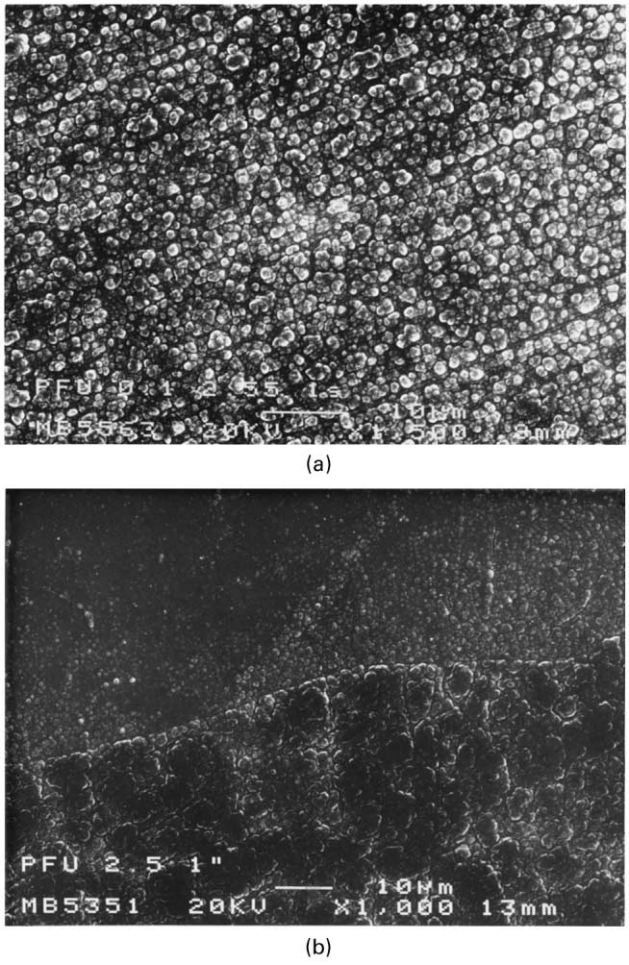

Fig. 5. Scanning electron micrographs of some growth layers of A_1 films from different zones.

first electropolymerisation second, $t_p = 1$ s, showed different shades of grey indicating irregular growth and covering; some zones were thicker than others. The growth of the deposit began at the edges and spread towards the centre. Fig. 5 shows images of the initial deposits of A_1 films. These were formed by interlinked nodular structures oriented 45° to the longitudinal axis of the electrode. This level of order has been observed in PFu/ClO_4 films synthesised in different synthesis conditions and higher t_p [26]. The nodule sizes were carefully determined to avoid the interpenetrated ones (Fig. 5a). The lowest area and perimeter found were 0.65 μm^2 and 2.54 μm, respectively, (see Table 1). The Kolmogorov–Smirnov test [27] showed that a normal distribution function could be assumed for these magnitudes. It is interesting to notice that there are several growth levels even in the first second of electropolymerisation, and therefore different thicknesses. This confirmed that while nucleation was taking place over some parts of the electrode, the film grew faster over the previously formed nuclei.

Fig. 5b shows the limit zone of the growth. There are two well delimitated layers. The lower part of the micrograph corresponds to more developed growth that spreads over the first layer formed (top part of the image). The nodule size of this top part is quite similar to the one in Fig. 5a, however, the lower zone presents larger nodules due to a more highly developed growth process. There are also links among them. As we move away from the centre to the upper edge of the electrode, the lower electrode zone is also covered by a PFu/ClO_4 film with different growth levels (although nodule size is nearly half of the other).

It is interesting to note that platinum electrodes were not subjected to any prior treatment that could give rise to any specific orientation. The nuclei had an oriented growth and the PFu/ClO_4 chains were aligned following a direction parallel to the substrate, from the first second, similar to polypyrrole [28].

As t_p increased to 4 s, the growth over the electrode evolved to the central zone. The nodule size increased strongly from A_1 to A_4 films, maintaining it almost constant from $t_p = 4$ s to higher electropolymerisation times (Table 1). It is interesting to point out that there are more interlinked nodules giving groups of larger size (4.3 ± 0.6 μm^2 and 7.2 ± 0.6 μm). In these A_4 films, dendritic structures appeared, producing the perpendicular growth detected in other synthesis conditions at higher t_p [26]. These dendritic structures (Fig. 6) consist of a concentric circular growth on the nodule structure. This indicates a change in the film growth from parallel to perpendicular to the electrode surface. These circles are also formed by strongly joined nodules, which in some cases appear as a single group. The size of these concentric circles decreases as we move away from the electrode surface. These dendritic formations

Table 1
Nodule size characteristics in films depending on t_p: area (a), perimeter (p) and maximum (d_{max}) and minimum (d_{min}) diameter of PFu/ClO_4 films and nodule numbers per unit area (N° of nod/μm^2)

t_p	a (μm^2)	p (μm)	d_{max} (μm)	d_{min} (μm)	N° of nod/μm^2
1	0.66±0.03	2.65±0.22	1.14±0.06	0.78±0.05	1.51
4	1.29±0.09	3.84±0.17	1.49±0.06	1.14±0.05	0.77
10	1.04±0.10	3.48±0.20	1.40±0.08	0.99±0.05	0.96
358	1.06±0.09	3.46±0.17	1.42±0.06	1.00±0.05	0.94
600	1.19±0.07	3.79±0.13	1.54±0.06	1.06±0.04	0.84
1800	1.61±0.12	4.36±0.20	1.74±0.08	1.25±0.05	0.62
4400	1.45±0.12	4.10±0.19	1.65±0.07	1.17±0.06	0.69
6000	1.53±0.13	4.20±0.19	1.63±0.07	1.22±0.06	0.65

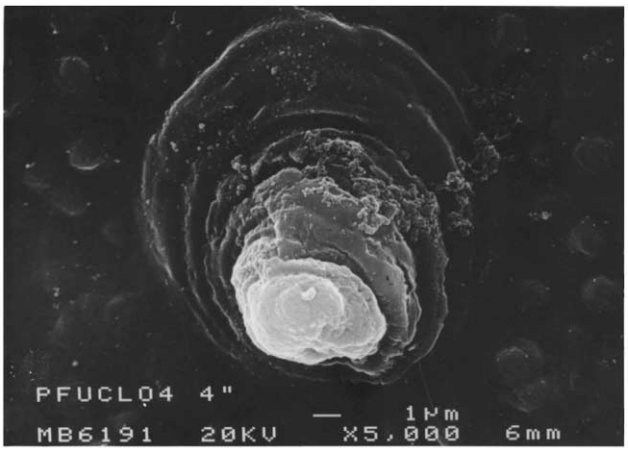

Fig. 6. Scanning electron micrograph of the dendritic structure of A_4 films.

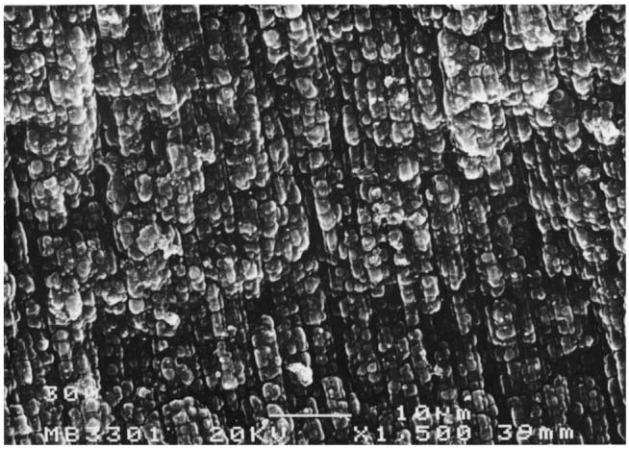

Fig. 7. Scanning electron micrograph of the growth face of A_{358} films.

are distributed throughout the film structure at this t_p. In Table 2, we have shown the area, a, and perimeter, p, of the concentric circles that formed the dendritic structure; n is a number assigned to each circle to identify them, that is, $n = 1$ is the circle of larger size, where the growth of the dendrite begins, and $n = 9$ represents the farthest circle of the film surface, the little one.

As the electropolymerisation time was increased, $t_p = 10$ s, the covering of the electrode continued, maintaining the ordered nodular structure, the nodule size and the presence of dendrites. The dendrites detected at this t_p value had a higher size than the ones obtained at $t_p = 4$ s. This indicates that there was a continuous incorporation of nodules to the concentric circles as the film formation took place. Some different growth levels were also detected. The electropolymerisation had to be continued until 358 s to completely cover the electrode; then it was possible to analyse their cross-section and back face.

A_{358} films showed an ordered nodule structure with a nodule size similar to that of A_{10} films (Fig. 7 and Table 1). There were some lines where growth did not occur, creating discontinuities in the material and therefore some roughness. The back face, in contact with the electrode during growth, was smoother and homogeneous.

Some transversal fractures of A_{358} films were observed (Fig. 8). The inner structure was composed of interlinked nodular layers with some cavities between them. These images of film cross-sections again suggested the existence of an additional factor contributing to the film roughness produced by the alternating planar and normal growth of the film. Electrochemical studies confirm this three-dimensional growth [6]. The pores were irregular. Nearly 60% of the pores were in the range: $0.05 \leq a \leq 1\ \mu m^2$ and $2.0 \leq p \leq 6.0\ \mu m$. The area was not higher than $4\ \mu m^2$ except for two pores (arrowed in Fig. 8) that had values of 12.5 and $6.6\ \mu m^2$. The growth was therefore irregular, and slower in some zones than in others.

Fig. 9 shows the roughness profile of both A_{358} film faces, where e and d are the thickness and the analysed distance, respectively. It can be seen with the naked eye that the back face (Fig. 9b) is smoother; the bigger jump observed in Fig. 9b corresponds to a small crack. Nevertheless, the growth face presented some differences greater than

Table 2
Area (a) and perimeter (p) of the circle that formed the dendritic growth observed in A_4 films in Fig. 6, n is a number assigned to each circle from 1 to 9 being the nearest and the farthest circle from the film surface, respectively

n	a (μm^2)	p (μm)
1	121.07	39.88
2	77.17	31.63
3	58.60	27.43
4	35.72	21.95
5	26.54	18.68
6	11.73	12.64
7	5.55	8.59
8	3.42	6.82
9	0.18	1.64

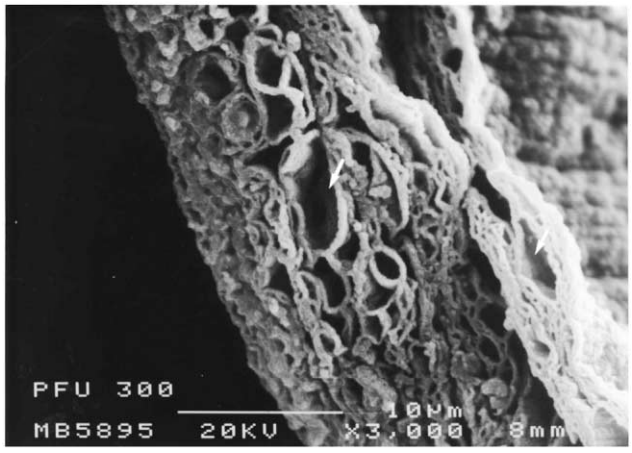

Fig. 8. Scanning electron micrograph of a cross-section of A_{358} PFu/ClO_4 films.

35 μm between consecutive points (Fig. 9a), because some zones grew faster. A homogeneous thickness could not therefore be estimated. We can only talk of the thickness per cm^2 as this changed from one zone to other, even between points close together in the same zone. The faster film growth was responsible not only for the different film roughness and growth levels over the previous nuclei layer, but also for the inner structure consisting of pores among layers. This made it difficult to measure the thickness by pressing the film surface with a needle.

The analysis of films synthesised at higher electropolymerisation times, $t_p > 358$ s, revealed no important differences in any of the sections studied. The nodule sizes were quite similar. At $t_p > 358$ s the nodule size increased slightly untill $t_p = 1800$ s. At $t_p > 1800$ s the nodule size diminished, but at longer times, this value remained more or less constant (see Table 1). At lower t_p, the nodules were better defined. The roughness increased with time. Differences of thickness greater than 60 μm between successive points were found; in some cases these differences were outside the range limit. The roughness measured in a perpendicular direction to the longitudinal axis of the electrode was greater than in a parallel direction.

Cross sections showed internal laminar structures similar to the ones synthesised at the lower t_p but more compact (see Figs. 8 and 10). As t_p increases, so does the number of layers, but the pores between them diminish. Apparently, there is a laminar structure with less well-defined pores.

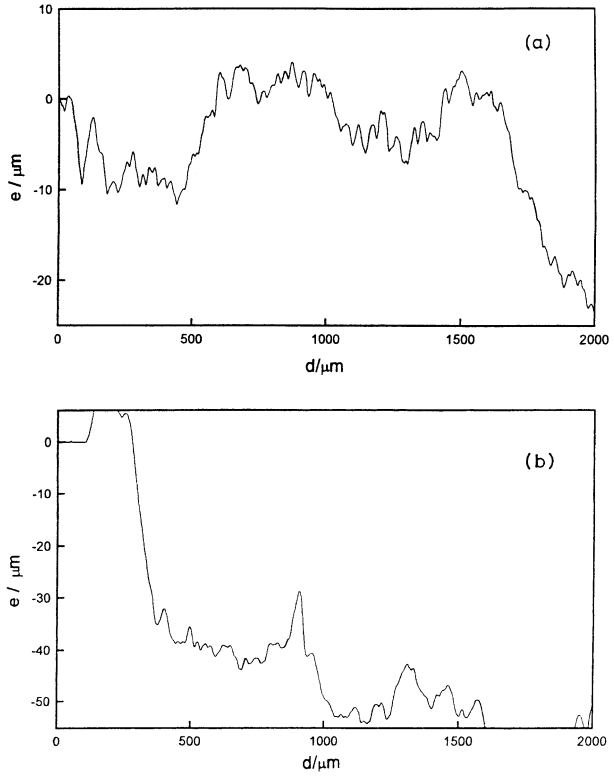

Fig. 9. Roughness profile of both faces of A_{358} films. (a) Growth face, (b) Back face.

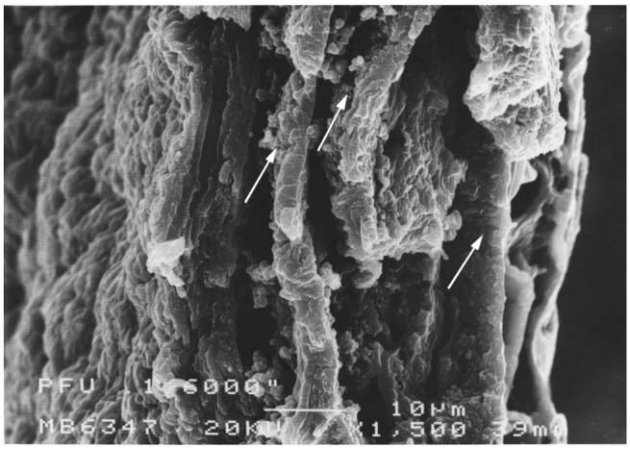

Fig. 10. Scanning electron micrograph of the cross-section of A_{6000} films.

Some intermediate layers formed by nodules are visible (see arrows in Fig. 10).

4. Conclusions

As noted in the Introduction, the electropolymerisation time is a very important parameter in the layered structure of conducting polymers, and therefore in PFu/ClO_4 films, because of the technological applications of these materials. Their structure (compact or non-compact), their nucleation mechanism, and the aromaticity linked to the π-conjugated system and hence to the conductivity, all provide important information.

Analysis of the influence of t_p on the synthesis of PFu/ClO_4 films reveals that in the early stages of electropolymerisation, the generation of active nuclei was favoured; however, as t_p increased, the formation rate of the polymer films remained almost constant.

There was three-dimensional growth of hemispherical nuclei, controlled by diffusion, with a mixture of instantaneous and progressive nucleation mechanisms, being the progressive contribution more prevalent.

FTIR spectra of all films revealed some changes on the film structure with t_p. The presence of a ring rupture is confirmed by the OH stretching vibration band, however, these films presented some aromaticity. This aromaticity increased with t_p until 1800 s and decreased for higher t_p values.

The generation of the first nuclei was very quick from the first second of synthesis; there were different nodular layers of growth and also some overlapping nodules. An ordered nodular structure in the growth face was detected from the first second of synthesis and persisted up to a longer t_p. The nuclei grew at 45° to the longitudinal axis of the electrode; the PFu/ClO_4 pores were aligned parallel to the substrate from the first seconds. The nodule size was better defined and increased with t_p.

At $t_p = 4$ s, some dendritic structures appeared, indicating

hat at shorter t_p, the films were less homogeneous. The nodules acquired constant dimensions from $t_p = 4$ s on. No important differences in morphology were found as t_p increased, with the exception of better nodule definition and increased roughness.

The cross sections analysed were formed by a laminar structure consisting of interconnected nodular layers. The film became more compact as the electropolymerization time increased.

Acknowledgements

This work has been partially supported by the DGES, under project PB97-0271. We wish to thank Dr J. Fernando Barbero for his assistance with the MATHEMATICA program used to fit our data.

References

[1] Cordova R, del Valle MA, Arratia A, Gómez H, Schreber RJ. Electroanal Chem 1994;377:75–83.
[2] Downard AJ, Pletcher D. J Electroanal Chem 1986;206:147–52.
[3] Asavapiriyanot S, Chandler GK, Gunawardena GA, Pletcher D. J Electroanal Chem 1984;177:229–44.
[4] Hoier SN, Parl SM. J Electrochem Soc 1990;140:2454.
[5] Otero TF, Rodriguez J. Electrochim Acta 1994;39:245–53.
[6] González-Tejera MJ, Carrillo Ramiro I, Hernández-Fuentes I. Electrochim Acta 2000;45:1973–82.
[7] Marcos ML, Rodríguez J, González-Velasco. J Electrochim Acta 1987;32:1453–9.
[8] Scharifker B, García-Pastoriza E, Marino W. J Electroanal Chem 1991;300:85–98.
[9] Kim YT, Collins RW, Vedam K, Allare DL. J Electrochem Soc 1991;138:3266–75.
[10] Hamnet A, Hillman AR. J Electrochem Soc 1988;135:2517–24.
[11] Chao F, Costa M, Tian C. Synth Met 1993;53:127–47.
[12] Randriamaharaka H, Noël V, Chevrot C. J Electroanal Chem 1999;472:103–11.
[13] Bade K, Tsakova V, Schultze JW. Electrochim Acta 1992;37:2255–61.
[14] Cai LT, Yao SB, Zhou SM. Acta Chim Sin 1995;53:1150–1.
[15] Soubiran P, Aeiyach S, Lacaze PC. J Electroanal Chem 1991;303:125–37.
[16] Asavapiriyanot S, Chandler GK, Gunawardena GA, Pletcher D. J Electroanal Chem 1984;177:245–51.
[17] González-Tejera MJ, Carrillo I, Hernández-Fuentes I. Synth Met 1998;92:187–95.
[18] González-Tejera MJ, Carrillo I, Hernández-Fuentes I. Synth Met 1995;73:135–40.
[19] Carrillo I, Barba C, González-Tejera MJ, Hernández-Fuentes I. Macromolecules 1996;29:5585–9.
[20] Carrillo I, González-Tejera MJ, Hernández-Fuentes I, Barba C. Solid State Commun 1995;95:107–10.
[21] Schrebler R, Grez P, Cury P, Veas C, Merino M, Gómez H, Córdova R, del Valle MA. J Electroanal Chem 1990;430:77–90.
[22] Thirsk HR, Harrison A. A guide to the study of electrode kinetics. Orlando: Academic Press, 1972. Chapter 3.
[23] Sánchez de la Blanca E, Carrillo I, González-Tejera MJ, Hernández-Fuentes I. J Polym Sci Part A Polym Chem 2000;38(2):291–8.
[24] Evans JC. Spectrochim Acta 1960;16:994.
[25] Colomban Ph, Gruger A, Novak A, Régis A. J Mol Struct 1994;317:261.
[26] Carrillo I, González-Tejera MJ. Polym Int 2000;49:1565–71.
[27] Press WH, Flannery BP, Teukolsky SA, Vetterling WT. Numerical recipes in C. The art of scientific computing. USA: Cambridge University Press, 1988.
[28] Montemayor MC, Vázquez L, Fatás E. J Apply Phys 1994;75:1849–51.